We are IntechOpen, the world's leading publisher of Open Access books
Built by scientists, for scientists

6,900
Open access books available

186,000
International authors and editors

200M
Downloads

154
Countries delivered to

Our authors are among the

TOP 1%
most cited scientists

12.2%
Contributors from top 500 universities

CLARIVATE ANALYTICS
BOOK CITATION INDEX
INDEXED
WEB OF SCIENCE™

Selection of our books indexed in the Book Citation Index
in Web of Science™ Core Collection (BKCI)

Interested in publishing with us?
Contact book.department@intechopen.com

Numbers displayed above are based on latest data collected.
For more information visit www.intechopen.com

Microemulsion Method for Synthesis of Magnetic Oxide Nanoparticles

A. Drmota[1], M. Drofenik[2,3], J. Koselj[1] and A. Žnidaršič[1,2]
[1]Nanotesla Institute Ljubljana
[2]CO NAMASTE
[3]Faculty of Chemistry and Chemical Engineering
Slovenia

1. Introduction

Among many of known nanomaterials, the special position belongs to magnetic nanoparticles, which are fundamentally differing from the classic magnetic materials with their domain structure. The magnetic properties of nanoparticles are determined by many factors, such as chemical composition, type and degree of defectiveness of the crystal lattice, particle size and shape, morphology (for structurally inhomogeneous particles), interaction of the particle with the surrounding matrix and the neighboring particles (Gubin, 2009). For this reason, it is important to develop techniques by which the size, shape and chemical homogeneity of the particles can be well controlled (Hessien et. al., 2008). Numerous nonconventional techniques, such as precipitation in aqueous solutions (Pankov et. al., 1993), glass crystallization method (Sato & Umeda, 1993), self-propagating high-temperature synthesis method (Elvin et. al., 1997), hydrothermal method (Ataie et. al., 1995), mechanical alloying (Ding et. al., 1998) and the sol-gel method (Surig et. al., 1994), were used to prepare magnetic nanoparticles.

Among them, a precipitation in microemulsion has been shown as a perspective method for the preparation of magnetic nanopartqicles of controlled size and morphology (Košak et. al., 2004).

A microemulsion can be defined as a thermodynamically stable isotropic dispersion of two immiscible liquids consisting of nanosized domains of one liquid in the other, stabilized by an interfacial film of surface-active molecules. The surfactant molecules provide a confinement effect that limits particle nucleation, growth and agglomeration. In this method, co-precipitation occurs in tiny droplets of water ("water pools") embedded with surfactant molecules and homogenously distributed in an oil phase. The size of these "water pools", so called reverse micelles, which act as micro reactors for the synthesis of the nanoparticles, is thermodynamically defined by the water-to-surfactant molar ratio (R) (Makovec & Košak, 2005).

Although there are many kinds of interesting magnetic nanoparticles, we have been focused our study on iron oxide nanoparticles.

First of all, we synthesized silica (SiO_2) coated maghemite (γ-Fe_2O_3) nanoparticles. Monodisperse magnetic nanoparticles with unique properties, which are dominated by

superparamagnetism, have a great potential to use in biomedical applications such as cell labeling and magnetic cell separation, drug delivery, hyperthermia and MRI contrast enhancement due to of their non-toxic nature and lower susceptibility to physical and chemical changes. In this field the main challenge is to create the suitable surface of magnetic nanoparticles in order to functionalize and allow strong interactions with specific biological components. Therefore, chemical modification of the nanoparticle surface with biocompatible molecules, such as silica (SiO_2), dextran, polyvinyl alcohol (PVA) and phospholipids, is an important issue that provides bio functionality and resistance to physiological conditions such as pH and enzymes, binding sites between the particles and the target sites on the cell, cytotoxic drug attaching to a biocompatible magnetic nanoparticle carrier, etc. Superparamagnetic nature and a high degree of specific magnetization of these magnetic nanoparticles are demanded for their applications in drug delivery or magnetic separation to defeat hydrodynamic forces acting on the nanoparticles in the flowing solution. Small sizes are required to allow the transport through the vascular system or tisular diffusion of particles (Mornet et. al., 2002; Vidal-Vidal et. al., 2006).

On the other hand, we have been focusing our study on M-type strontium hexaferrite ($SrFe_{12}O_{19}$) nanoparticles because of their magnetoplumbite structure, which present a high magnetization and strong magnetic anisotropy along c axis. Such properties of material, which are directly related to crystallographic structure, are very important because of their use in the manufacture of microwave-absorbing materials. The development of novel electromagnetic (EM) wave absorption materials has great interest. Although, electric equipments make our life more convenient, the electromagnetic (EM) radiation restricted the continual development of our society because of their pollution to environment and harm to human beings.

The absorption of EM waves occurs in magnetic materials due to their magnetic losses (Lax & Button, 1962). Ferrites with a submicron grain size are some of the most promising materials in magnetic nanocomposites for the absorption of microwave radiation (Bregar, 2004). In nanocomposite form a ferrite can be used for the absorption of microwave radiation where the ferromagnetic nanopowders exhibit a higher absorption at low field strengths and a broader absorption range in the microwave region than multi-domain powders.

Ferrites exhibit substantial magnetic losses in the vicinity of their natural resonance (FMR). Because of this phenomenon they are one of the best materials for MW absorbers. Ferrites with a spinel crystal structure can be applied in the frequency range of several hundred MHz to several GHz (Pardavi Horvath, 2000). AM_2O_4 spinel ferrites are binary ferromagnetic oxides with compositions in the system Fe_2O_3–MO, where M is usually a transition element. Almost any divalent transition-metal ion can be replaced to form spinel ferrite. However, magnetite is an exceptional case, where the M is Fe^{2+}. The spinel ferrite's cubic unit cell comprises eight formula units with 16 M^{3+} cations on 16 octahedral sites and $8M^{2+}$ ions on the tetrahedral A sites. In the reversed spinel eight of 16 M^{3+} ions occupy all the tetrahedral sites. The magnetic properties of ferrites can be considered in terms of the Neel model of ferrimagnetism. One of the good properties of ferrites is the possibility to prepare different compositions and thereby modify the magnetic properties.

On the other hand, ferrites with a hexagonal structure are an extensive family of compounds with a complex magnetoplumbite structure within the ternary system AO–Fe_2O_3–MeO, where A = Ba, Sr, Ca(La) and Me is a bivalent transition metal. Due to their high natural

frequency, these ferrites can be used across the whole GHz region (Pardavi Horvath, 2000). Furthermore, these ferrites do not require external bias fields in RF operation and are "self-biased" due to their very high intrinsic anisotropy and can be applied for the miniaturization of microwave devices (Ovtar et. al., 2011). Their operating range is around the remanence of the rectangular hysteresis loop. Due to the solely Fe^{3+} state in the hexaferrite lattice, they are good insulators with very low dielectric losses. The best-known members are the uniaxial permanent magnets of the M-type, i.e., Ba and Sr-hexaferrites, which can be used across the whole GHz region (Rodrigue, 1963).

By varying the chemical compositions, it is possible to control the electromagnetic properties such as the saturation magnetization, magnetocrystalline anisotropy, permeability and the permittivity of a ferrite composite. In addition, the microstructure of ferrites has an additional impact on their properties, and consequently on the EM absorption. Compared to the ferrites with a spinel structure, the hexagonal ferrites exhibit a larger intrinsic magnetocrystalline anisotropy field and it can be applied at higher frequencies. In general, MW absorbers can be prepared in the form of ceramics or as composites, where the ceramic phases are embedded in a polymeric matrix. Here, the EM properties of the composites can be very effectively tuned, simply by varying the volume fractions of the filler constituent phases.

In addition, a synergetic effect of the constituent phase properties may also be observed in some composites. For this reason magnetic composites are interesting for microwave applications (Kim et. al., 1994; Nakamura & Hankui, 2003; Pereira et. al., 2009; Verma et. al., 2002; Ghasemi et. al., 2008; Groningen, 2003). Furthermore, during the development of suitable absorbers, their composition and processing are equally important.

2. Experimental procedure

In the present investigation, silica (SiO_2) coated maghemite (γ-Fe_2O_3) nanoparticles were performed *in-situ* via the precipitation in two different microemulsion systems. First microemulsion system consisted from water phase (aqueous solution of Fe^{2+}/Fe^{3+} ions or aqueous solution of NH_4OH), sodium n-dodecyl sulfate (SDS) served as anionic surfactant, 1-butanol served as co-surfactant and cyclohexane used as an oil phase. The second microemulsion system consisted from water phase (aqueous solution of Fe^{2+}/Fe^{3+} ions or aqueous solution of NH_4OH), n-Hexadecyltrimethylammonium bromide (CTAB) served as cationic surfactant, 1-butanol served as co-surfactant and 1-heksanol used as an oil phase. Whatever of the chosen system, the synthesis of nanoparticles was performed at the same water-to-surfactant + co-surfactant molar ratio (R).

The influence of the concentration of reactants in aqueous phase, the temperature of reaction, the pH value after the precipitation of hydroxides and the type of surfactant and co-surfactant, on the maghemite (γ-Fe_2O_3) nanoparticles were investigated. The thickness of silica shell was carefully controlled by the amount of tetraethoxysilane (TEOS) added to the microemulsion after the precipitation step.

The precursors of strontium hexaferrite ($SrFe_{12}O_{19}$) were prepared with the classical co-precipitation method and with the microemulsion method in microemulsion system water/SDS, 1-butanol/cyclohexane. The precursors were calcined at different

temperatures ranging from 400 °C to 1000 °C in air. The influence of the Sr^{2+}/ Fe^{3+} molar ratio and the calcination temperature on the product formation and magnetic properties were studied.

Furthermore, the composites based on the magnetic filler, composed of phases within the SrO - Fe_2O_3 system, embedded in the polyphenylene sulfide (PPS) matrix with a concentration range of 80:20 by weight destined for microwave absorption were investigated. The electromagnetic parameters of composites were measured with a vector network analyzer at 400 MHz – 32 GHz.

2.1 Synthesis of silica (SiO_2) coated maghemite (γ -Fe_2O_3) nanoparticles

The chemical reagents used in this synthesis process were iron (II) sulfate heptahydrate ($FeSO_4$ $7H_2O$, ACS, 99+%), iron (III) sulfate hydrate ($Fe_2(SO_4)_3$ xH_2O, Reagent Grade), ammonium hydroxide solution (25%, puriss p.a.), sodium n-dodecyl sulfate (SDS) ($CH_3(CH_2)_{11}OSO_3Na$, Fluka, 99%), n-Hexadecyltrimethylammonium bromide (CTAB) ($CH_3(CH_2)_{15}N(Br)(CH_3)_3$, Alfa Aesar, 99+%), 1-Butanol ($CH_3(CH_2)_3OH$, Alfa Aesar, 99%), cyclohexane (C_6H_{12}, ACS, Alfa Aesar, 99+%), 1-hexanol ($CH_3(CH_2)_5OH$, Alfa Aesar, 99%), tetraethoxysilane (TEOS) ($Si(C_2H_5O)_4$, Alfa Aesar, 98%) and ethanol (CH_3CH_2OH, Riedel-de Haën, 96%).

Maghemite (γ-Fe_2O_3) nanoparticles were prepared according to Schikorr´s reaction, eq 1 (Košak et. al., 2004):

$$Fe^{2+} + Fe^{3+} + 2OH^- + O_2 \rightarrow \gamma\text{-}Fe_2O_3 + H_2O \tag{1}$$
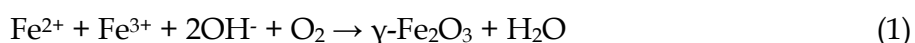
In this synthesis, the Fe (II) and Fe (III) hydroxides were precipitated during the reaction between two different microemulsions containing an aqueous solution of corresponding ions (MEI) or precipitating reagent (MEII). In the second step of the synthesis, the Fe (II) hydroxide is oxidized, resulted to the formation of the spinel maghemite (γ-Fe_2O_3) phase. The surface of γ-Fe_2O_3 nanoparticles prepared in microemulsion systems was functionalized with tetraethoxysilane (TEOS).

Synthesized SiO_2 coated γ-Fe_2O_3 nanoparticles were characterized using transmission electron microscopy (TEM), X-ray diffractometry (XRD) and specific surface area measurements (BET). The specific magnetization (DSM-10, magneto-susceptometer) of the prepared samples was also measured.

2.1.1 Experimental procedure

Two aqueous solutions were prepared (aqueous solution of Fe^{2+}/Fe^{3+} ions (0.4 or 0.15 M) and 5 % aqueous solution of NH_4OH). Aqueous solution of Fe^{2+}/Fe^{3+} ions with a molar ratio 1.85:1 was prepared by dissolving an appropriate amounts of iron (II) sulphate heptahydrate, $FeSO_4 \cdot 7H_2O$, and iron (III) sulphate hydrate, $Fe_2(SO_4)_3$ xH_2O.

To chose a suitable composition that formed stable water-in-oil (w/o) microemulsion in the systems:

- water/SDS, 1-butanol/cyclohexane (System A) and
- water/CTAB, 1-butanol/1-hexanol (System B).

The region of microemulsion stability, within which the microemulsion is optically transparent was determined by the titration method in connection with conductivity measurements. In Fig. 1 the microemulsion stability region for both systems is represented by solid line for 0.4 M aqueous solution of Fe^{2+}/Fe^{3+} ions and by dashed line for 5 % aqueous solution of NH_4OH, within which the compositions of microemulsion are optically transparent. These are pseudo-ternary phase diagrams, in which every point represents a quaternary system whose overall composition is entirely defined by any pair among the three weight fractions: f_w (aqueous phase), f_s (surfactant + co-surfactant) and f_o (oil phase).
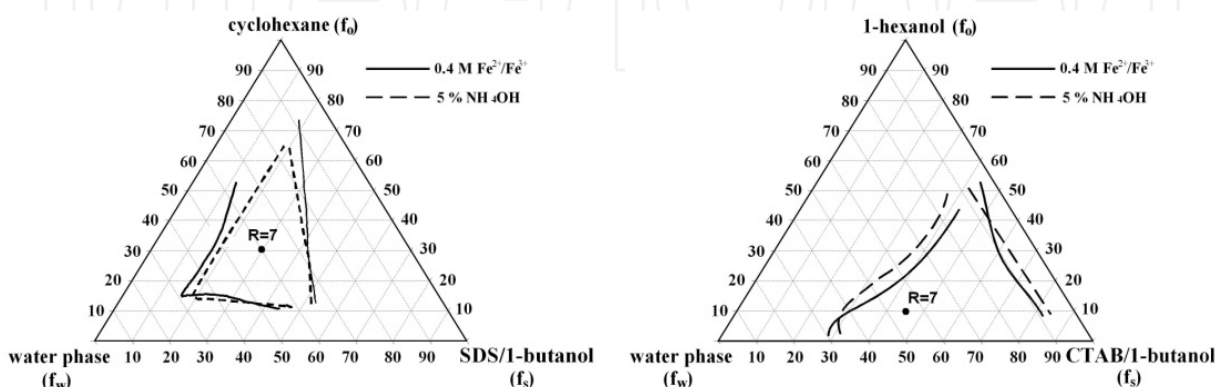

Fig. 1. Phase diagram of the water / SDS / 1-butanol / cyclohexane system (left) and water/CTAB, 1-butanol/1-hexanol (right) at 20 °C.

Prior to the synthesis, two microemulsions of the same composition were prepared. The microemulsion I (MEI) contained 0.4 M or 0.15 M aqueous solution of Fe^{2+}/Fe^{3+} ions, whereas the microemulsion II (MEII) contained 5 % aqueous solution of the ammonium hydroxide (NH_4OH) served as precipitation agent. The SDS to 1-butanol (System A) and CTAB to 1-butanol (System B) weight ratios were kept constant at 1:1.3 and 1.5:1, respectively. In the second step, MEI and MEII were mixed at different temperatures and different pH values for 1 h. A black precipitate was formed immediately. In the last step, the surface of γ-Fe_2O_3 nanoparticles prepared in microemulsion systems with the same molar ratio (R=7) and the following composition for system A: 39 wt. % of water phase, 31 wt. % of SDS/1-butanol, 31 wt. % of cyclohexane and for the system B: 45 wt. % of water phase, 10 wt. % of CTAB/1-butanol, 45 wt. % of 1-hexanol was functionalized using TEOS. The thickness of silica shell was carefully controlled by the amount of TEOS added to the microemulsion after the precipitation step. Finally, the product was centrifuged and washed several times with mixture of ethanol and water and dried at 100 °C.

2.1.2 Results and discussion

Fig. 2 shows the X-ray diffraction patterns of the prepared samples. Except in the case of sample S2 (pH = 6), the diffractograms confirmed the formation of the spinel structure, characteristic of magnetite (Fe_3O_4) and maghemite (γ-Fe_2O_3) with different Fe^{2+} content. The chemical analysis of the synthesized nanoparticles showed that they contain only around 0.5 wt. % of Fe^{2+}. From this we confirmed the formation of γ-Fe_2O_3 nanoparticles.

To estimate the average particle size (D_{XRD}) a Debye-Scherrer formula was used. The values are shown in Table 1.

The difference in the XRD patterns is in the broadness of the peaks. Broader peak indicates smaller crystallite size. From the graph, it is observed that the crystallite size for sample S1 is the smallest one and it is followed by samples S6, S4, C7, C8, C9 and S3, respectively. With increasing the concentration of aqueous solution of Fe^{2+}/Fe^{3+} ions from 0.15 M to 0.4 M the average size of the nanoparticles increased from 5.6 nm to 7.5 nm (samples S6 and S4), and with increasing the reaction temperature from 20 °C to 50 °C, the average size of the nanoparticles increased from 3.3 nm to 7.3 nm (samples S1 and S4). The pH value had a strong influence to average particle size and phase composition. At pH 6 a non-magnetic phase was formed (what about the magnetic properties of the products obtained in other pH conditions?). With increasing of the pH value from 8.6 to 10.2, the average size of the nanoparticles decreased from 12.8 nm to 7.3 nm (samples S3 and S4).

System	Sample	MEI (M)	$T_{(syn.)}$ (°C)	$pH_{(syn.)}$	BET (m^2/g)	D_{BET} (nm)	D_{XRD} (nm)	M (Am^2/kg)
A	S1	0.4	20	10.2	226	5.4	3.3	19
	S2		50	6.0	132	9.3	-	1.4
	S3		50	8.6	100	12.2	12.8	49
	S4		50	10.2	189	6.5	7.3	48
	S5		50	10.4	213	5.8	-	31
	S6	0.15	50	10.2	274	4.5	5.6	14
B	C7	0.4	20	9.5	102	12.0	7.6	51
	C8	0.4	50	9.5	92	13.3	8.8	60
	C9	0.15	50	9.5	101	12.2	8.8	52

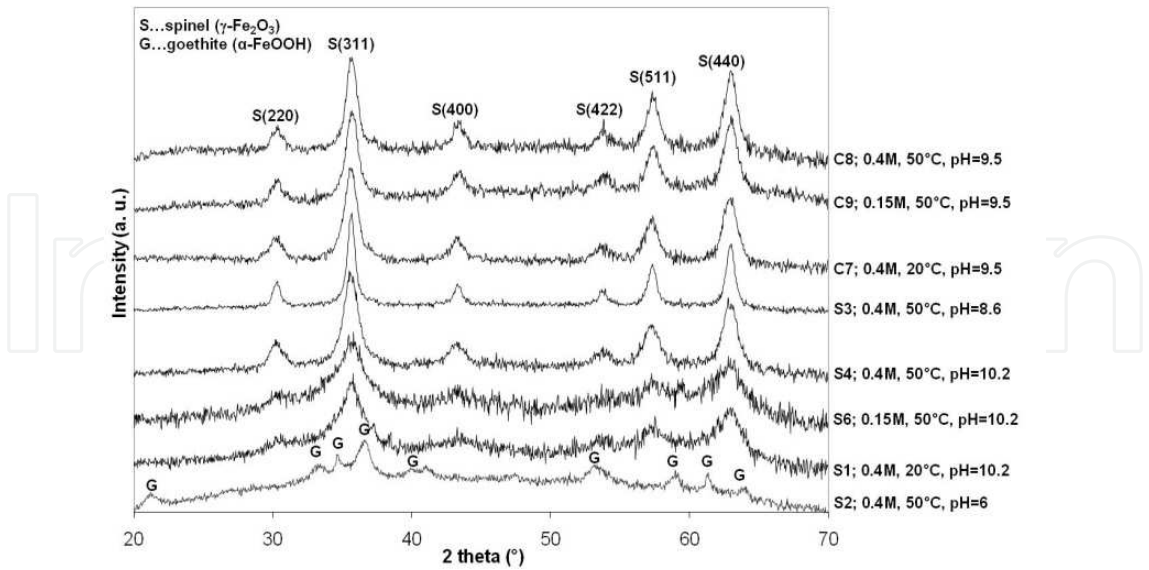Table 1. Influence of preparation conditions on the properties of prepared samples.

Fig. 2. XRD patterns of synthesized samples.

Fig. 3 left shows TEM image of uncoated γ-Fe_2O_3 nanoparticles, which were spherical in shape and highly agglomerated, in compare to the γ-Fe_2O_3 nanoparticles obtained after the surface coating (Fig. 3 right) with a thin layer of SiO_2.

The results show that the concentration of Fe^{2+}/Fe^{3+} ions in aqueous solution , the reaction temperature and the pH value had a strong influence on the average particle size distribution and as a consequence on the specific magnetization.

The results in Table 1 show that with decreasing of concentration of Fe^{2+}/Fe^{3+} ions in aqueous solution from 0.4 M to 0.15 M, the average particle size determined from BET measurements decreases from 6.5 nm to 4.5 nm in system A (samples S4 and S6) and from 13.3 nm to 12.2 nm in system B (samples C8 and C9). The smallest average particle size was obtained at 20 °C. With increasing of the reaction temperature from 20 °C to 50 °C, the average particle size increased from 5.4 nm to 6.5 nm in system A (samples S1 and S4) and from 12 nm to 13.3 nm in system B (samples C7 and C8). At pH 6 a nonmagnetic phase was formed with the average particle size of 9.3 nm and a specific magnetization of 1.4 Am^2/kg (system A, sample 2). With increasing the pH value from 8.6 to 10.3 in system A, the average particle size decreased from 12.2 nm to 5.8 nm (samples S3, S4 and S5).
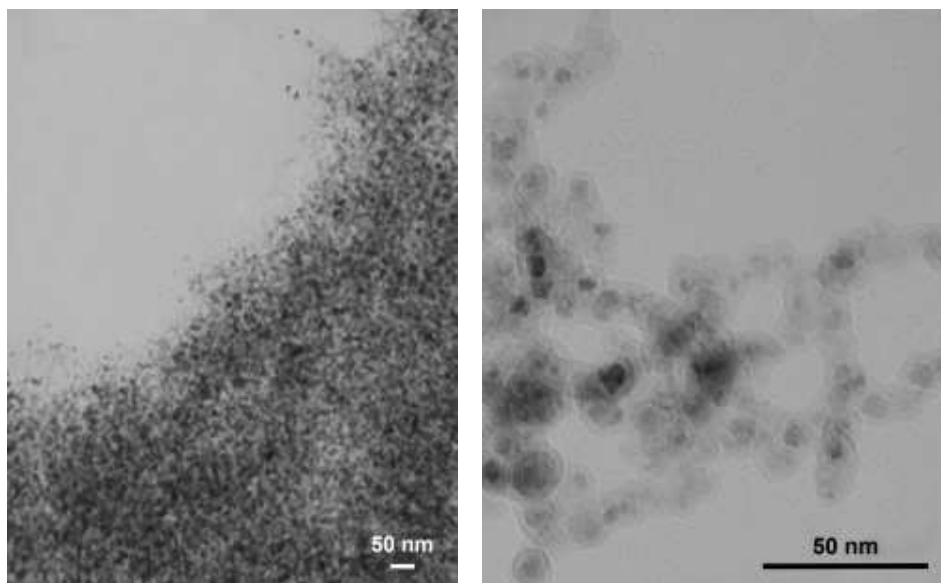

Fig. 3. TEM micrograph of (left) uncoated γ-Fe_2O_3 nanoparticles and (right) γ-Fe_2O_3 nanoparticles obtained with a thin layer of SiO_2.

Fig. 4 shows that specific magnetization (M) of the prepared γ-Fe_2O_3 nanoparticles increased from 19 Am^2/kg for the sample with average particle size of 5.4 nm (system A, sample S1) to 49 Am^2/kg for the sample with average particle size 12.2 nm (system A, sample S3) and from 51 Am^2/kg for the sample with average particle size 12 nm (system B, sample C7) to 60 Am^2/kg for the sample with average particle size 13.3 nm (system B, sample C8).

The thickness of silica shell was carefully controlled by the amount of TEOS added to the microemulsion mixture during the precipitation step. Specific magnetization of the uncoated γ-Fe_2O_3 nanoparticles prepared in microemulsion system A, was 48 Am^2/kg (sample S4) and decreased to 25 Am^2/kg for the nanoparticles with 3 nm thickness of silica shell (Fig. 5). Furthermore, the specific magnetization of the uncoated γ-Fe_2O_3 nanoparticles prepared in microemulsion system B was 60 Am^2/kg (sample C8) and decreased to 21 Am^2/kg, when the thickness of silica shell was 4 nm (Fig. 5).
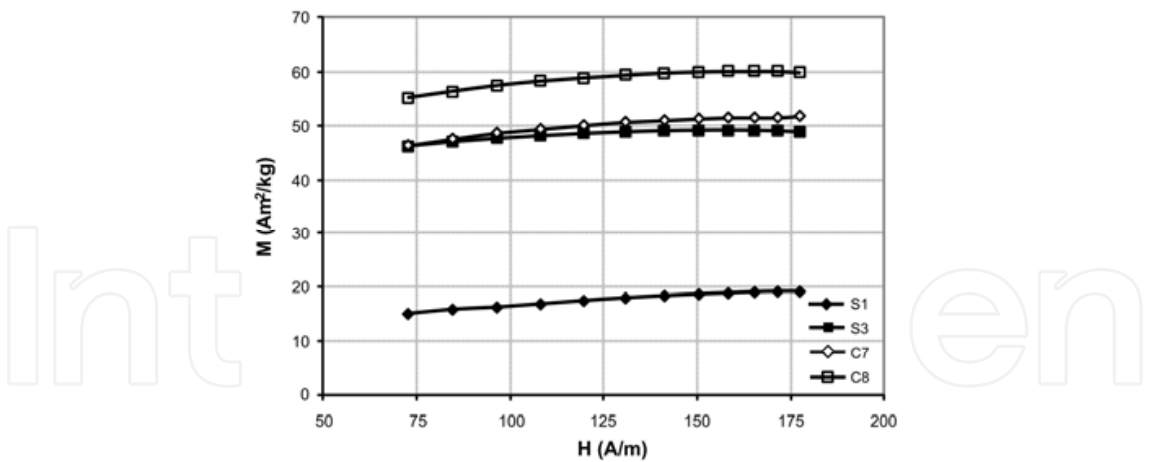
Fig. 4. Specific magnetization of uncoated γ-Fe₂O₃ nanoparticles prepared in microemulsion systems water / SDS / 1-butanol / cyclohexane (samples S1 and S2) and water/CTAB, 1-butanol/1-hexanol (samples C7 and C8).
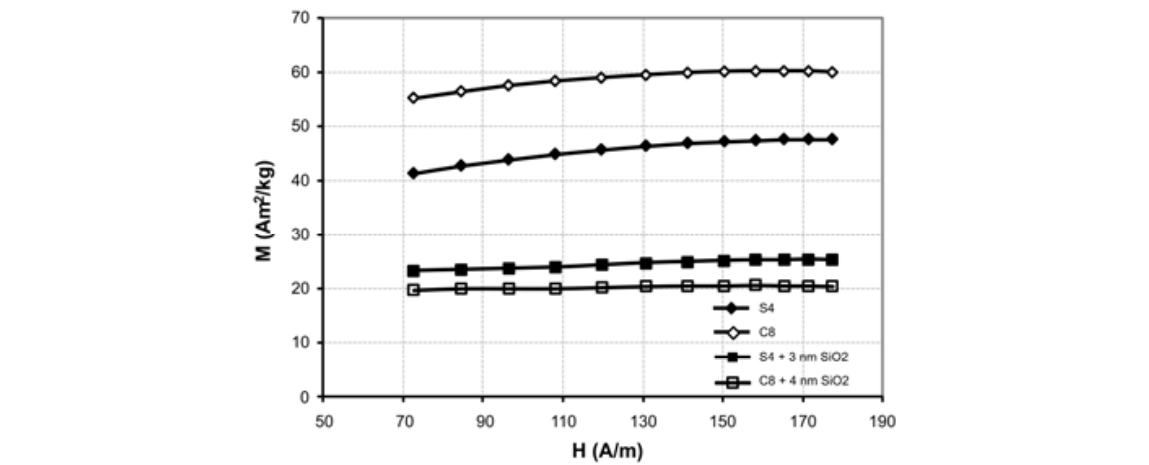

Fig. 5. Specific magnetization of uncoated and coated γ-Fe₂O₃ nanoparticles prepared in microemulsion systems water / SDS / 1-butanol / cyclohexane (samples S4 and S4 + 3 nm SiO₂) and water/CTAB, 1-butanol/1-hexanol (samples C8 and C8 + 4 nm SiO₂).

2.2 Synthesis of strontium hexaferrite SrFe₁₂O₁₉ nanoparticles

The chemicals used for the syntheses of the different samples were strontium nitrate anhydrous ($Sr(NO_3)_2$), 98%, Alfa Aesar, iron (III) nitrate nonahydrate ($Fe(NO_3)_3 \cdot 9H_2O$), ACS, 98,0-101,0%, Alfa Aesar; tetramethylammonium hydroxid solution 25% (TMAH) ($C_4H_{13}NO$), Applichem; cyclohexane (C_6H_{12}), ACS, 99+%, Alfa Aesar; sodium n-dodecyl sulfate (SDS) ($CH_3(CH_2)_{11}OSO_3Na$), 99%, Sigma Aldrich; 1-butanol ($CH_3(CH_2)_3OH$), 99%, Alfa Aesar and ethanol (CH_3CH_2OH), 96%, Riedel-de Haën.

The precursors of strontium hexaferrite ($SrFe_{12}O_{19}$) were prepared according to the reaction, eq 2:

$$Sr(NO_3)_2 + 12Fe(NO_3)_3 + 38(CH_3)_4NOH \rightarrow Sr(OH)_2 + 12\,Fe(OH)_3 + 38((CH_3)_4N)NO_3 \quad (2)$$
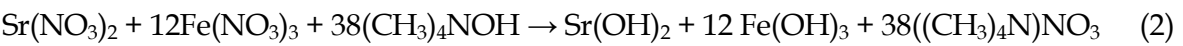
In this synthesis, the Sr (II) and Fe (III) hydroxides were precipitated during the reaction between two different aqueous solutions or microemulsions containing an aqueous solution of corresponding ions (MEI) and precipitating reagent (MEII). In the second step of the synthesis, the hydroxides are oxidized during the calcinations process, resulting in the formation of the nano-crystalline hexagonal ($SrFe_{12}O_{19}$) phase according to the reaction, eq 3:

$$Sr(OH)_2 + 12Fe(OH)_3 \rightarrow 6Fe_2O_3 + SrO + 19H_2O \qquad (3)$$

The dried precursors were characterized using thermogravimetric analyses (TGA) and differential thermal analyses (DTA) in air with a heating/cooling rate of 5 °C/min. The morphology of the powders after the calcination was investigated with transmission electron microscopy (TEM). The size of the nanoparticles was measured with dynamic light-scattering particle size analyses (DLS) and from the powders specific surface area A_s using the BET method and estimated using the relation $D_{BET} = 6\rho/A_s$ where $\rho = 5.1$ g/cm^3 for spherical particles. The magnetic measurements of the calcined samples were carried out using a magneto-susceptometer (DSM-10).

2.2.1 Experimental procedure

The co-precipitation and the microemulsion methods were applied for the preparation of the $SrFe_{12}O_{19}$ precursors. Prior to the synthesis, aqueous solutions of strontium and iron nitrate with various Sr^{2+}/Fe^{3+} molar ratios (1:6.4, 1:8, 1:10 and 1:12) were prepared. Although a molar ratio of 1:12 should be sufficient, according to the stoichiometry, an excess of strontium nitrate was necessary, because the strontium hydroxide is partially soluble in water (Ataie, 1995).

In the co-precipitation method the Sr(II) and Fe(III) hydroxide precursors were precipitated during the reaction between the aqueous solution of metal nitrates and the 0.5 M aqueous solution of tetramethylammonium hydroxide (TMAH), which served as a precipitating agent (Table 2). The precipitation was performed at room temperature and a pH value of 12.7. The brownish precipitates were washed several times with a mixture of distilled water and ethanol (volume ratio 1:1) and dried at 100 °C.

	Aqueous solution	wt. %
Metal nitrates	0.01 M $Sr(NO_3)_2$ + 0.08 M $Fe(NO_3)_3$	50
Precipitating agent	0.5 M TMAH	50

Table 2. The composition of a typical co-precipitation system used for the synthesis of the precursor with a Sr^{2+}/Fe^{3+} molar ratio of 1:8.

The microemulsion system used in this study consisted of sodium n-dodecyl sulfate (SDS) as the surfactant, 1-butanol as the cosurfactant, cyclohexane as the continuous oil phase and an aqueous solution of reactants as the dispersed phase. Two microemulsions (I and II) with identical compositions and different reagents in the aqueous phase were prepared (Table 3). The aqueous phase in microemulsion I comprised of a mixture of strontium and iron nitrate aqueous solutions. The aqueous phase in microemulsion II comprised of a 0.5 M solution of tetramethylammonium hydroxide (TMAH), which served as a precipitation agent. The brownish precipitates of metal hydroxides appeared within the nanosized aqueous droplets

after the two microemulsions were mixed at room temperature and pH 13.5. The precipitates were washed several times with a mixture of distilled water and ethanol (volume ratio 1:1) and dried at 100 °C.

Finally, these dried precursor powders prepared with different Sr^{2+}/Fe^{3+} molar ratios were calcined at different temperatures (400 to 1000 °C) for 1h with a heating/cooling rate of 5 °C/min. The calcinations were performed in a sample holder in the TG apparatus in a static atmosphere with a precise control of the weight change and the calcination temperature.

	Microemulsion I	Microemulsion II	wt. %
Aqueous phase	0.01 M $Sr(NO_3)_2$ + 0.08 M $Fe(NO_3)_3$	0.5 M TMAH	35
Surfactant	SDS	SDS	13
Cosurfactant	1-butanol	1-butanol	17
Oil phase	cyclohexane	cyclohexane	35

Table 3. The composition of the microemulsion system used for the synthesis of the precursor with a Sr^{2+}/Fe^{3+} molar ratio of 1:8.

2.2.2 Results and discussion

Typical TGA and DTA curves of the dried precursors prepared with the co-precipitation method and the microemulsion method at a Sr^{2+}/Fe^{3+} molar ratio of 1:8 are shown in Fig. 6.

The DTA thermograms of the samples prepared by the co-precipitation method show an endothermic peak at 116 °C and two exothermic peaks at 262 °C and 719 °C. The endothermic peak was attributed to the vaporization of the water from the precursor. On the other hand, the first exothermic peak was ascribed to the disintegration-oxidation of the residual organic precipitation agent in air at elevated temperatures. The second exothermic pick was attributed to the formation enthalpy and/or subsequent crystallization of the hexaferrite ($SrFe_{12}O_{19}$).

In the case that the precursor was prepared by co-precipitation in a microemulsion, the DTA thermograms indicated an endothermic peak at 116 °C and three exothermic peaks at 255 °C, 288 °C and 735 °C. Here, the endothermic peak is a consequence of the vaporization of the residual solvent and the water from the precursor. While the appearance of two close but separate exothermic peaks between 255 °C and 288 °C is consistent with the chosen method of synthesis, where we used two different organic agents, i.e., in addition to an organic precipitation agent (TMAH), an organic surfactant (SDS) was also employed. However, both of them exhibited different disintegration temperatures. The third exothermic peak at around 735 °C could, like in the former case, be attributed to the formation of crystalline $SrFe_{12}O_{19}$.

The TGA showed a continuous weight loss from room temperature to about 730 °C. Theoretically, the transformation of the dried precursor hydroxides $Sr(OH)_2$ and $Fe(OH)_3$ into their oxides SrO and Fe_2O_3 and further into the hexagonal ferrite structure, at a Sr^{2+}/Fe^{3+} molar ratio of 1:8, during the calcination in air led to a weight loss of around 24%, which is in good agreement with the experimental results (Fig. 6).

In order to investigate the effect of the calcination temperature on the formation of $SrFe_{12}O_{19}$ powders, co-precipitated samples and those prepared in microemulsions was calcined at various temperatures, ranging from 600 to 1000 °C, for a precursor Sr^{2+}/Fe^{3+} molar ratio of 1:6.4. Figs. 7 and 8 show the XRD patterns of these samples.
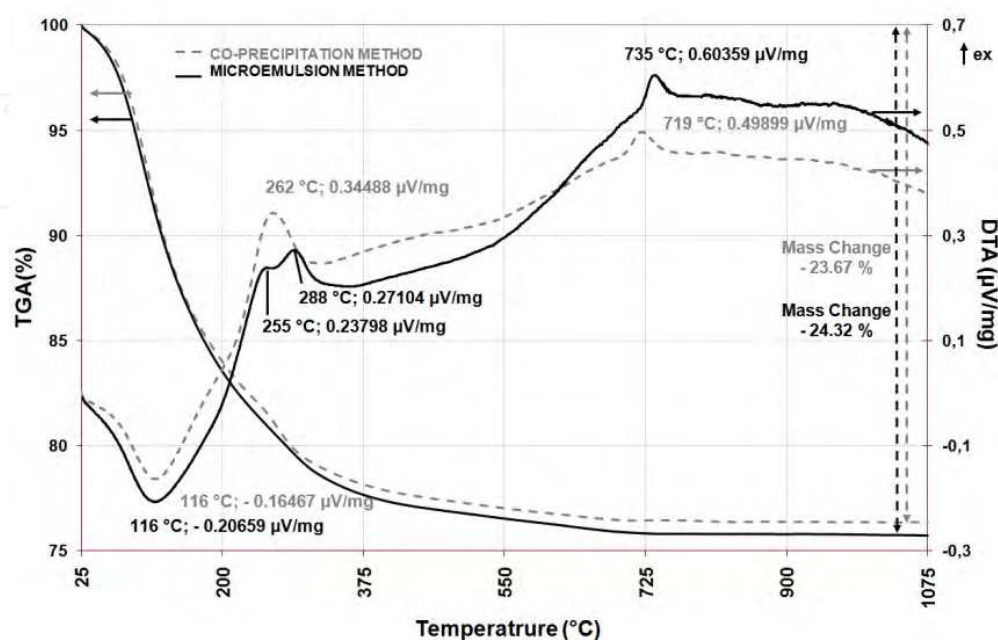

Fig. 6. DTA and TGA thermograms of precursor with the Sr^{2+}/Fe^{3+} molar ratio 1:8 prepared by the co-precipitation and microemulsion methods.

The XRD patterns of the produced powders showed the presence of strontium hexaferrite $SrFe_{12}O_{19}$, strontium peroxide SrO_2, hematite Fe_2O_3, and magnetite Fe_3O_4 phases depending on the calcination temperature and the method of synthesis.

At a low temperature of 600 °C, powder prepared by co-precipitation contained a nonmagnetic phase hematite Fe_2O_3, while the powder prepared with the microemulsion method contained the magnetic phase magnetite. Here, the temperature to form the Sr-hexaferrite is too low, while on the other hand, the second constitutive phase SrO is, in spite of its large excess at low calcinations temperatures, not observed due to its low crystallinity.

The formation of two different forms of iron oxides during the calcinations at 600 °C, i.e., hematite after the co-precipitation was used and magnetite when the microemulsion method was applied can be explained by the difference in the preparation method. The precipitation reaction should be slower in a reverse micelle medium, when considering the necessary coupling of the rate constant of the chemical reaction and the rate constant of the fusion of the reverse micelles, which must happen prior to the particular reaction (Natarajan et. al., 1996).

The slower rate of the precipitation, when the synthesis is performed within the reverse micelles, which leads to a compartmentalization of the bulk compared to that in the bulk conditions, could lead to the formation of $Fe_2O_3\ H_2O$, which on further heating might yield a magnetic phase maghemite/magnetite. However, the main condition that is crucial for the formation of magnetite is the presence of organic aids, which during heating at elevated temperatures prior to the complete oxidation and the formation of

carbon oxide, ensures the reduction conditions that yield the magnetite phase instead of the hematite. Furthermore, the reaction occurs in a closed system of the TGA apparatus, where any draught of air was excluded. On the other hand, in co-precipitated and calcined samples the $Fe(OH)_3$ yields hematite.

At a temperature of 800 °C it is mainly the formation of $SrFe_{12}O_{19}$ that can be observed for both types of samples, prepared by co-precipitation and/or by microemulsion-assisted synthesis. This is consistent with the DTA, where the maximum assigned to ferrite formation is observed at 735 °C. Besides, some XRD peaks of hematite Fe_2O_3 in the samples prepared via microemulsion the hematite phase can be detected.

The XRD analysis of the samples calcined at 900 °C showed the formation of the $SrFe_{12}O_{19}$ phase, with no other phase being detected, Figs. 7 and 8. This sample still has a large excess of SrO and the temperature is sufficiently high that all of the hematite and/or magnetite in the precursor reacts to form the hexaferrite phase, with the exception of the strontium oxide, which was designed to be in excess due to the partial solubility of the strontium hydroxide in the water/alcohol during the processing of the precursor. The SrO, which is otherwise prone to react with atmospheric moisture and carbon dioxide, forming hydrocarbonates with a low crystallinity, can be easily extracted with dilute hydrochloric acid and chemically analyzed, while the Sr-hexaferrite is poorly soluble in acids. From these results one can conclude that the Sr^{2+}/Fe^{3+} molar ratio of 1:6.4 is a little bit too high, since the excess of free SrO and/or SrO_2 can be chemically analyzed in the calcined samples.

On the other hand, the XRD patterns for the samples calcined at 1000 °C show identical diffraction patterns to those of the samples calcined at 900 °C. Therefore, one can conclude that the calcination temperature at 900 °C is sufficient for a complete reaction between stoichiometric ratios of the precursor components forming the target phase, i.e., $SrFe_{12}O_{19}$, while the excess of SrO can be easily removed from the product.

In order to complete the range of trial-and-error experiments the samples with Sr:Fe molar ratios of 1:8, 1:10 and 1:12 were calcined at 900 °C. Here, the influence of a relatively large excess of SrO in the precursor was gradually reduced and the phase formation depending on the calcinations temperature was followed by XRD (Fig. 9) and by measuring the magnetization of the products (Figs. 12 and 13).

Fig. 9 shows the XRD patterns for the samples prepared with the co-precipitation method and Sr^{2+}/Fe^{3+} molar ratios of 1:6.4, 1:8, 1:10 and 1:12. The pure crystalline single-phase $SrFe_{12}O_{19}$ was formed at a Sr:Fe molar ratio of 1:6.4. On the other hand, the XRD patterns of the produced samples at Sr^{2+}/Fe^{3+} molar ratios of 1:8, 1:10 and 1:12 showed, besides strontium peroxide SrO_2, the presence of the magnetite Fe_3O_4 phase.

With a decrease of the relatively large excess of Sr^{2+} the magnetite phase starts to appear, as observed from the XRD spectra and the magnetization measurements, Fig. 12. It is surprising that in spite of an overall large excess of SrO in the precursor the iron oxide phases can be detected in calcined samples with a molar ratio > 1:6.4. The magnetite Fe_3O_4 phase in the samples to a great extent determines the magnetic properties, as is clear from the hysteresis curves, Fig. 13. The phase compositions for the samples prepared with the microemulsion method were almost the same. The proposed reason for such a diverse phase formation, depending on the Sr^{2+}/Fe^{3+} molar ratio, is discussed latter.
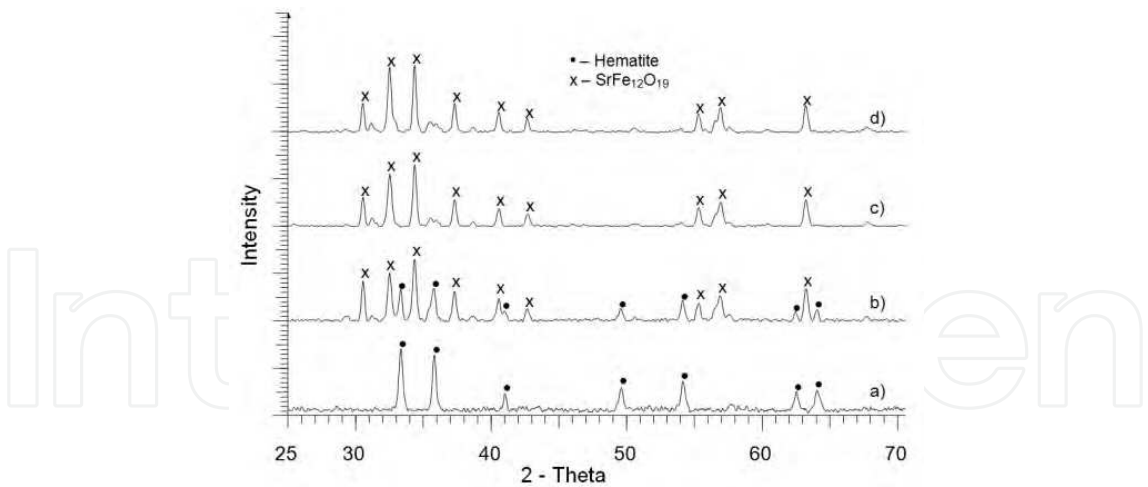
Fig. 7. XRD patterns of co-precipitated samples with a Sr^{2+}/Fe^{3+} molar ratio of 1:6.4 calcined at temperatures: a) 600 °C, b) 800 °C, c) 900 °C and d) 1000 °C for 1h.
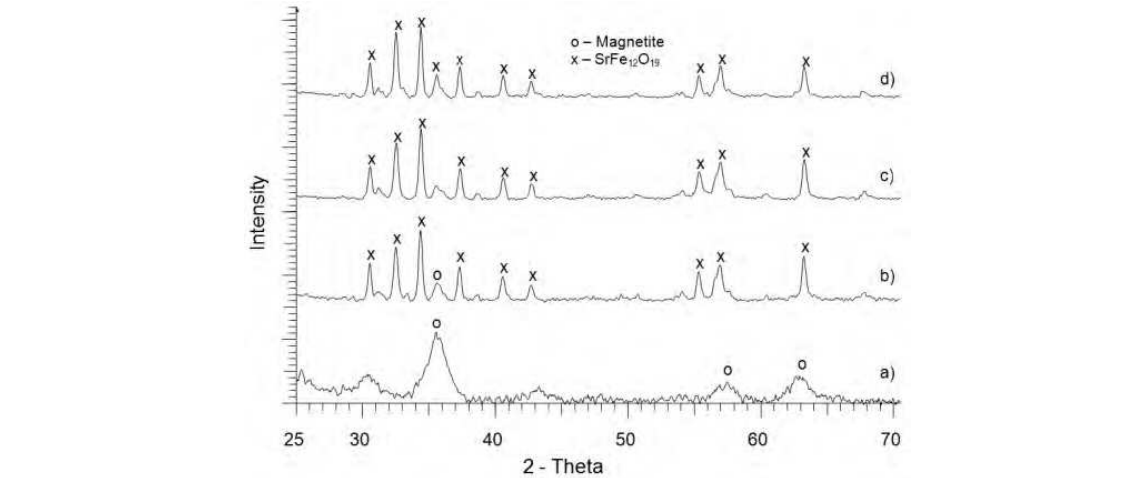

Fig. 8. XRD patterns of samples prepared by the microemulsion method with a Sr^{2+}/Fe^{3+} molar ratio of 1:6.4 calcined at temperatures: a) 600 °C, b) 800 °C, c) 900 °C and d) 1000 °C for 1h.
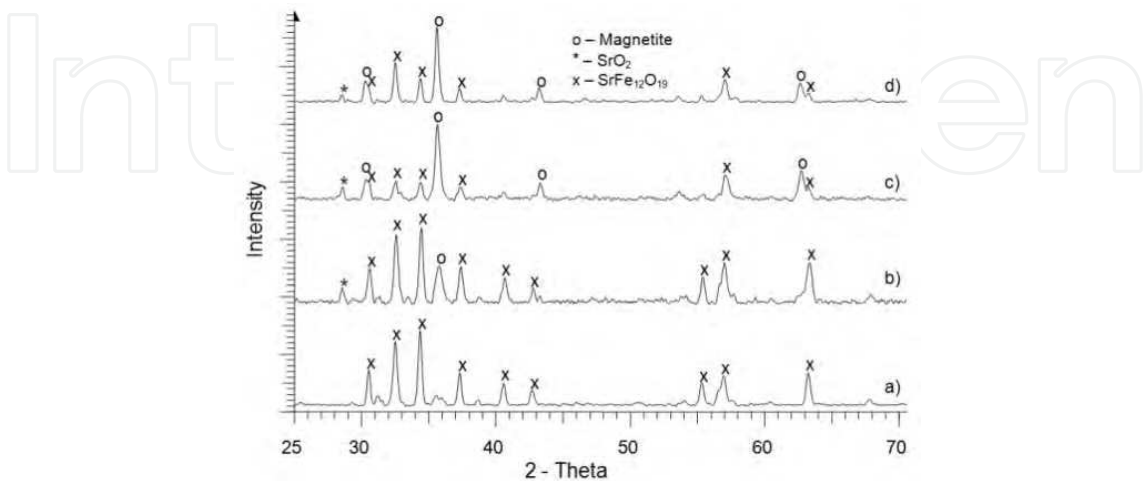

Fig. 9. XRD patterns for samples with various Sr^{2+}/Fe^{3+} molar ratios: a) 1:6.4, b) 1:8, c) 1:10 and d) 1:12) prepared with the co-precipitation method calcined at 900 °C.

Figs. 10 and 11 show the TEM images of $SrFe_{12}O_{19}$ particles prepared by the co-precipitation and microemulsion methods, respectively, with a Sr^{2+}/Fe^{3+} molar ratio of 1:8, calcined at 900 °C for 1h. There were no dramatic differences in both of the particle size and morphology when the samples were prepared using different synthesis methods.

The average size of the $SrFe_{12}O_{19}$ particles in the samples with a limited degree of agglomeration is in the range of 40–80 nm, from an inspection of the TEM images. However, when we compare this value with that of the average particle size obtained from the BET measurements, i.e., the d_{BET} = 61 nm (19 m²/g) with the same Sr^{2+}/Fe^{3+} molar ratio, one can conclude that the agglomeration of particles during the processing is not remarkable. Namely, the agglomeration of the particles might strongly decrease the measured total surface area and consequently the average particle size estimated from it is apparently larger. The average size of the nanoparticles stabilized in a suspension, i.e., in butylene glycol using a sonificator, was also measured using a dynamic light-scattering particle size analysis (DLS). The results of the DLS analysis showed that the size of the nanoparticles was around 40 nm. Here we must stress that the high energy of the ultrasound radiation breaks the agglomerates and decreases their number. Taking into account the data from the TEM images, the DLS analyses and the BET measurements one can describe the morphology of the synthesized powders as being composed of mostly not agglomerated particles of a size around 40 to 80 nm. The critical diameter of a spherical strontium hexaferrite with a single domain is calculated using the eqs 4 and 5 (Rezlescu et. al., 1999):

$$D_{m(crit)} = 9\sigma_w/2\pi M_s^2, \tag{4}$$

where

$$\sigma_w = \sqrt{\left(\frac{2k_B T_c |K_1|}{a}\right)} \tag{5}$$

is the wall density energy, $|K_1|$ the magnetocrystalline anisotropy constant, T_c the Curie temperature, M_s the saturation magnetization, k_B the Boltzmann constant and a the lattice constant. For $D_m < D_{m(crit)}$ the particles are multi domains. For Sr-hexaferrite, using T_c = 749K, a = 5.88·10⁻⁸ cm, $|K_1|$ = 3.6·10⁶ erg/cm³ and M_s = 450 Gauss, the value of $D_{m(crit)}$ estimated was around 250 nm. Thus, all the strontium ferrite particles in this investigation are of single domain.
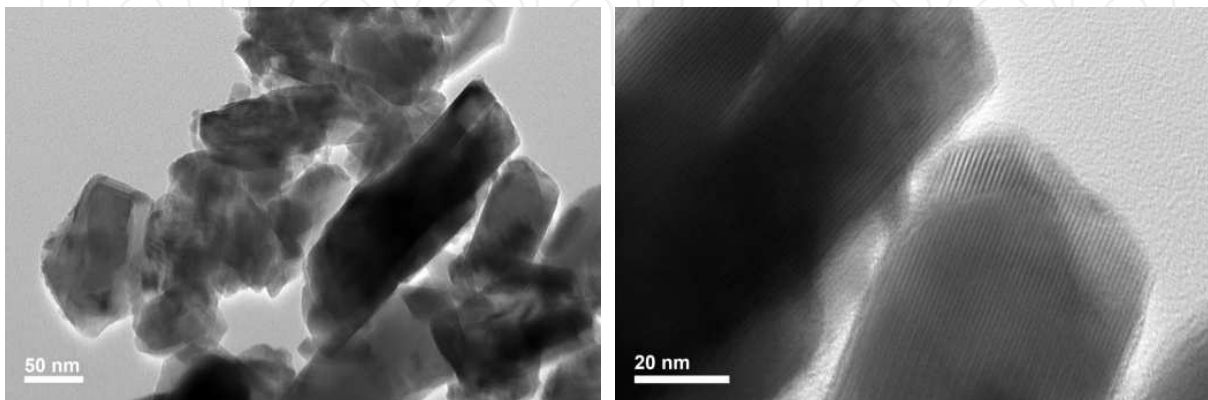

Fig. 10. TEM micrographs of $SrFe_{12}O_{19}$ prepared by the co-precipitation method and calcinated at 900 °C for 1 h.
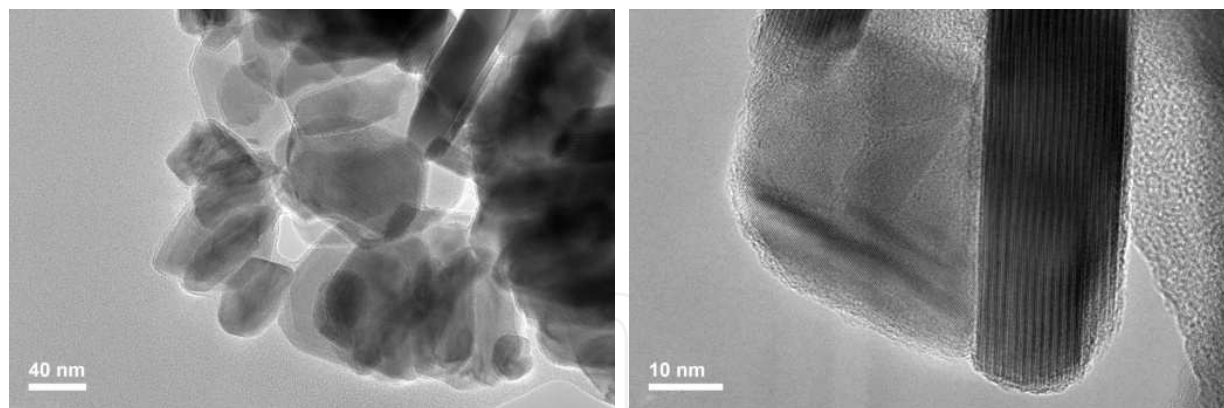
Fig. 11. TEM micrographs of $SrFe_{12}O_{19}$ prepared by the microemulsion method and calcinated at 900 °C for 1 h.

Therefore, we correlate the results of the magnetization measurements with the phase composition of the studied samples for a constant precursor Sr^{2+}/Fe^{3+} molar ratio heated at temperatures from 600 °C to 1000 °C. The saturation magnetization vs. calcination temperature for samples prepared by the co-precipitation and microemulsion methods, with a Sr^{2+}/Fe^{3+} molar ratio of 1:6.4 calcined at different temperatures for 1h is shown in Fig. 12. Following the magnetization of the product versus the temperature of the calcinations, we see a gradual increase of the magnetization, which is to be expected, according to the phase composition recorded with XRD spectra, Figs. 7 and 8. At 400 °C the low magnetization mostly reflects the composition of the precursor, where the ferrimagnetic phases were just starting to form, but could not be detected in the XRD spectra. They are, however, reflected in a slight magnetization. With an increase of the calcination temperature to about 600 °C the saturation magnetization increased from 4 Am^2/kg at 400 °C to 6 Am^2/kg in the case of the co-precipitation method, and from 10 Am^2/kg to 29 Am^2/kg at 600 °C for the samples prepared from microemulsions. With a further increase in the calcination temperature the magnetization steadily increases to 45 Am^2/kg for the co-precipitated samples and 55 Am^2/kg for the samples from the microemulsion. When the temperature increased to 900 °C and 1000 °C the magnetization of the magnetic particles stays in the range between 50 and 60 Am^2/kg.

The relatively large difference in the saturation magnetization for the co-precipitated and/or the microemulsion synthesized samples calcined at 600 °C are related to the phase composition of the powders examined by XRD analysis. The samples prepared with the co-precipitation method contained hematite, whereas those prepared with the microemulsion method contained the magnetic phase magnetite that increases the magnetization of the otherwise non-magnetic constitutive part (SrO) in the powder calcined at 600 °C. With a further temperature increase the target hexaferrite is being formed Figs. 7 and 8, which increases the magnetization of the calcined products.

Fig. 13 shows the plots of the saturation magnetization (M_s) as a function of the applied field (H_c) for samples prepared by the co-precipitation method and the microemulsion method with different Sr^{2+}/Fe^{3+} molar ratios and calcined at 900 °C for 1h. Here, the shape of the hysteresis loops indicates a drastic change in the phase composition depending on the precursor composition and the temperature.

The samples prepared with Sr^{2+}/Fe^{3+} molar ratios of 1:6.4 and 1:8 exhibited a relatively high saturation magnetization of 64 and 62 Am^2/kg, respectively, and wide hysteresis loops with coercivities of 5.4 and 5.0 kOe and remanent magnetizations of 39 and 36 Am^2/kg, respectively. With decreasing the Sr^{2+}/Fe^{3+} molar ratio from 1:8 to 1:10 and/or 1:12 the shape of the hysteresis loop changes drastically, indicating a crucial change in the phase composition, i.e., the magnetic properties of the samples change from high coercivity phases, indicating a hard magnetic character, to a soft magnetic phase. The XRD analysis indicates that the hard magnetic phase is Sr-hexaferrite and the soft magnetic phase is magnetite.

The formation of a submicron-sized strontium hexaferrite, responsible for a nearly square-shaped hysteresis loop in samples with a molar ratio Sr^{2+}/Fe^{3+} of 1:6.4 and 1:8, and a submicron-sized magnetite, exhibiting a hysteresis loop with a very small coercivity, indicating a soft magnetic character in samples with lower Sr^{2+}/Fe^{3+} molar ratios, 1:10 and 1:12, is consistent with the coarsening ability of fine, reactive, iron oxide particles. The essential element of this phenomenon is the fact that the coarsening of the iron particles occurs prior to the onset of the key solid-state reaction, which leads to the target compound. This process is associated with the passivity of the iron oxide particles due to a drastic decrease in the specific surface area needed for an effective solid-state reaction.

At molar ratios of 1:6.4 and 1:8 the solid-state reactions forming Sr-hexaferrites are straightforward, as is usually observed during the preparation of Sr-hexaferrites via a solid-state reaction. The large excess of SrO leads to a direct formation of the hexaferrite phase and can be easily extracted with dilute hydrochloric acid after the termination of the solid-state reaction.

However, at low molar ratios the course of the phase formation is widely different and is grounded on the well-known self-sintering phenomenon (Natarajan et. al., 1996). The soft magnetic particles of magnetite powder formed in that case represent the major part of the reaction product, exhibiting a hysteresis loop with a very low coercivity, Fig. 13. In addition, in these samples, with a low Sr^{2+}/Fe^{3+} molar ratio, the formation of $SrFe_{12}O_{19}$ at 750 °C, Fig. 6, is strongly hindered. The XRD diffraction spectra and the magnetic measurements show that magnetite is the major phase.

The observed phenomenon, i.e., with a large excess of Sr^{2+} the Sr-hexaferrite forms, while with a lower excess of Sr^{2+} mostly the iron oxides can be detected, can be linked to the high reactivity of the chemically synthesized iron oxide particles in the starting mixture. Such an otherwise homogeneous precursor mixture might favor, particularly at a low Sr^{2+}/Fe^{3+} molar ratio, the auto sintering of iron oxide powder (Urek & Drofenik, 1996), i.e., the coarsening of the reactive nanoparticles of iron oxide at a temperature lower than that needed to form Sr-hexaferrite at 750 °C, Fig. 6. This process is much more pronounced when the Sr^{2+}/Fe^{3+} molar ratio is low, where the coordination of the iron oxide particles with the same kind of particles is increased. The coarsening of the iron oxide particles leads to a drastic decrease in the iron oxide reactivity, inducing its passivity and strongly delaying the onset of the target solid-state reaction, the formation of Sr-hexaferrite.

Here, we recognize that in spite of the chemical method used in our studies the procedure by itself exhibits some peculiarities, which lead to the formation of unexpected phases.

During the preparation of fine-grained Sr-hexaferrite via chemical methods a large excess of SrO is required for the suppression of the auto sintering of iron oxide and represents a

general demand during the synthesis of iron-oxide-based compounds. Thus, in order to avoid the need for a large excess of SrO during the syntheses of fine-grained particles of Sr-hexaferrite the "*in-situ*" methods (Drofenik et. al., 2010) have an advantage over other chemical methods.
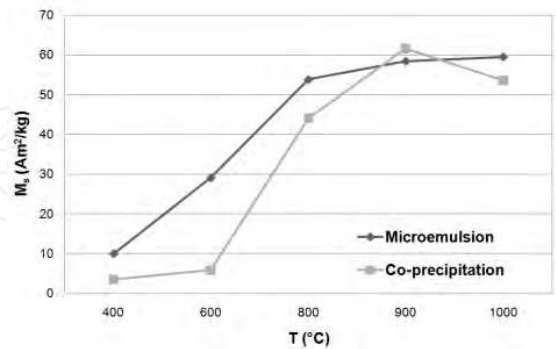

Fig. 12. The saturation magnetization (M_s) of samples prepared by the co-precipitation and microemulsion methods with Sr^{2+}/Fe^{3+} molar ratio 1:6.4 and calcined at different temperatures for 1h.
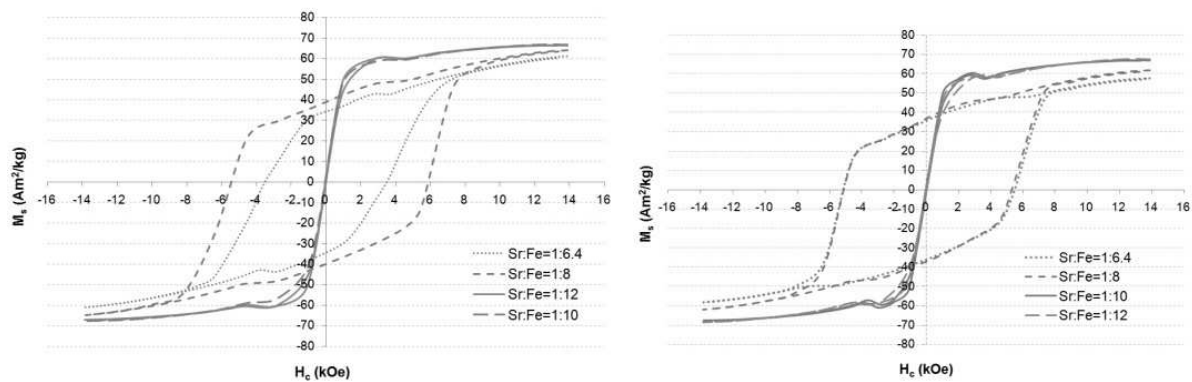

Fig. 13. The hysteresis loops of strontium hexaferrite prepared by the co-precipitation method (left) and the microemulsion method (right) with different Sr^{2+}/Fe^{3+} molar ratios and calcined at 900 °C for 1h.

The composite specimens for the measurement of the microwave-absorbing characteristics in the frequency range from 400 MHz to 32 GHz were prepared by mixing the magnetic powder and the PPS (Polyphenylene Sulfide) and pressing the mixture in an appropriate forming tool. The weight ratio of the magnetic powder and the PPS was 80:20, which gave a relatively high volume fraction of magnetic powder in the composite. The samples had a toroidal form with an inner dimension of 1.3 mm, an outer dimension 2.9 mm and a height of 1.3 mm, in order to fit well into the SMA[1] female or male adapter.

Both the relative complex permeability ($\varepsilon_r = \varepsilon'-j\varepsilon''$) and permittivity ($\mu_r = \mu'-j\mu''$) of the samples were measured using an Anritsu 37269D vector network analyzer in the frequency range from 400MHz to 32 GHz. The permeability and permittivity were calculated from the measured scattering parameters (Bregar et. al., 2007).

---

[1] SubMiniature version A.

The magnetic particles obtained via calcination, which serve as the magnetic/filler phase in the composites for the MW absorption, were magnetically characterized, as listed in Table 4.

The magnetization of sample S1 is 6 Am^2/kg, which is much higher than expected for hematite (α-Fe$_2$O$_3$), which at room temperature shows a weak magnetism of about 0.15 emu/g (Schieber, 1967). The observed magnetization of the sample is the result of the magnetic ingredients present in the product, which must consist of small amounts of maghemite and/or magnetite. These tend to form in small amounts as byproducts. Both of them contribute to the final magnetization of the sample, but they cannot be detected in the XRD pattern. However, when the powders are calcined at 800 °C and 900 °C, the particles changed from weakly magnetic to ferrimagnetic.

The saturation magnetization, remanent magnetization and coercivity increased with the calcination temperature from 38 Am^2/kg at 800 °C to 60 Am^2/kg at 900 °C. In sample S2 the magnetization increases due to the formation of Sr-hexaferrite phase. On the other hand, in sample S3, which consists of Sr-hexaferrite nanoparticles, the magnetization measured was 60 Am^2/kg, i.e., less than the bulk value (74.3 Am^2/kg). In part, the decrease in the magnetization of ultra-small nanoparticles can be attributed to their large surface-to-volume ratio and therefore the increased proportion of surface atoms that have an incomplete coordination leading to a non-collinear spin configuration (Kadama et. al., 1996).

The sample S4 consists of Sr-hexaferrite and magnetite. When considering the intensity of the diffraction peaks with the highest intensity it is possible to roughly estimate a mass ratio of 1:2 for the magnetite particles. The larger amount of magnetite in the composite contributes to a smaller coercivity and a lower remanent magnetization of the S4 sample. The results of the magnetic measurements are in agreement with the general principle that both phases with different magnetizations contribute to the final magnetization of the mixed product roughly in their mass proportions. Here, we have a mixture of a cubic magnetite phase, with soft magnetic properties, and a hexagonal ferrite, with hard magnetic properties, which in proportion to their mass ratios contribute to the average magnetization of the magnetic part of the composite in a magnetic field of 1T.

Sample code	Phase	Crystal structure	M_s (Am^2/kg)	M_r (Am^2/kg)	H_c (kA/m)
S1	α-Fe$_2$O$_3$	Cubic	6	/	/
S2	α-Fe$_2$O$_3$, SrFe$_{12}$O$_{19}$	Cubic, Hexagonal	38	25	399.4
S3	SrFe$_{12}$O$_{19}$	Hexagonal	60	36	464.2
S4	Fe$_3$O$_4$, SrFe$_{12}$O$_{19}$	Cubic, Hexagonal	63	7	15.4

Table 4. Magnetic assessment of the products investigated.

The complex permittivity ($\varepsilon_r' - j\varepsilon_r''$) and complex permeability ($\mu_r' - j\mu_r''$) are known to determine the absorption characteristics of the material. The real and the imaginary parts of the permeability of the composite specimens prepared for measurements of the microwave-absorbing characteristics in the frequency range from 400 MHz to 32 GHz with a weight ratio of magnetic powder to PPS = 80:20 are presented in Fig. 14. The real and the imaginary

parts of the permeability for samples S1, S2 and S3 are almost constant over the whole frequency range. Just the opposite is the case for sample S4, where the real part of the permeability rapidly decreased from 400 MHz to around 6 GHz, and after that it is lower than for the samples S2 and S3. The imaginary part of the permeability for sample S4 increases from 400 MHz to around 4.5 GHz, and after that it slightly decreases from 5 GHz to 25 GHz. These results are in an agreement with the theory (Giannakopoulou et. al., 2002; Feng et. al., 2007) that materials with a spinel structure (sample S4) have a higher permeability at lower frequencies than anisotropic materials with a hexagonal structure. Based on the fact that microwave absorbers must have a large imaginary part of the complex permeability, we can conclude that the specimens with a hexagonal structure, exhibiting just a notable imaginary part of permeability up to 32 GHz (samples S2 and S3), might be used as microwave-absorbing materials in the frequency range higher than 32 GHz.
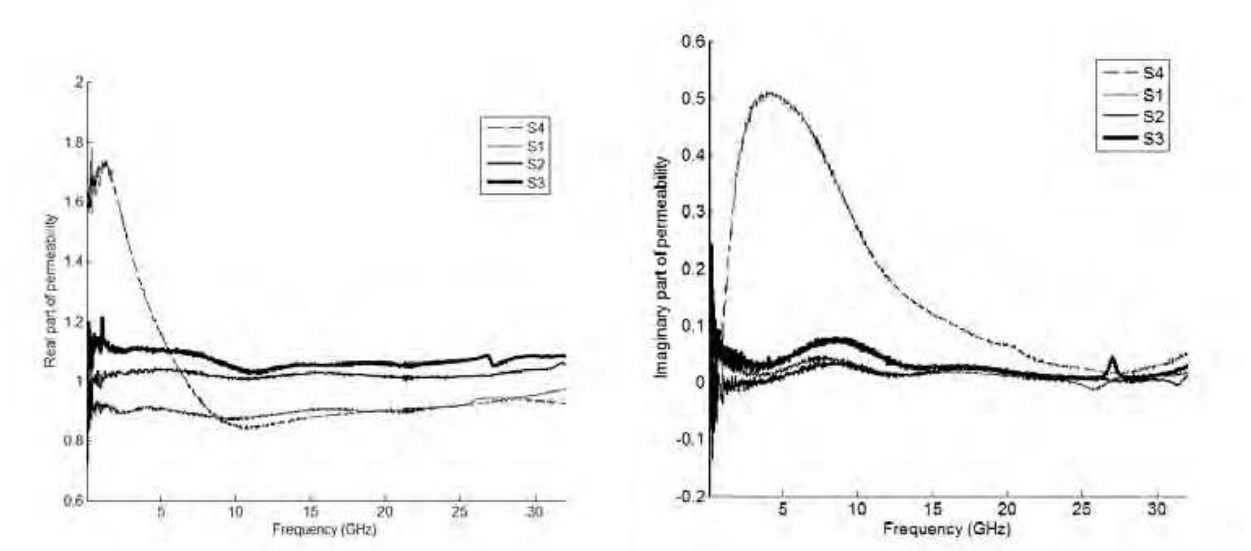

Fig. 14. The real (left) and imaginary (right) part of permeability of composites specimens with weight ratio magnetic powder:PPS = 80:20.

According to the transmission line theory, the reflection loss (RL) of electromagnetic radiation under normal wave incidence at the surface of a single/layer material backed by a perfect conductor can be given by (Ni et. al., 2010; Bregar & Žnidaršič, 2006):

$$R.L. = 20 log_{10} \left| \frac{Z_{in} - Z_0}{Z_{in} + Z_0} \right| \quad \text{unit: decibel (dB)} \tag{6}$$

where Z_0 is the characteristic impedance of free space,

$$Z_0 = \sqrt{\frac{\mu_0}{\varepsilon_0}} \tag{7}$$

and Z_{in} is the input impedance at free space and material surface:

$$Z_{in} = \sqrt{\frac{\mu_r}{\varepsilon_r}} tanh \left[j \left(\frac{2\pi f t}{c} \right) \sqrt{\mu_r \, \varepsilon_r} \right] \tag{8}$$

where μ_r and ε_r are the relative complex permeability and permittivity of the composite medium, respectively, which can be calculated from the complex scatter parameter, where c

is the velocity of light, f is the frequency of the incidence EW wave and t is the thickness of the composites. The impedance-matching condition is given by $Z_{in} = Z_0$, representing the ideal absorbing conditions.

Fig. 15 shows the dependence of the thickness of the absorber layer (d) on the reflection loss of the composite specimens with a weight ratio of the magnetic filler, i.e., PPS = 80:20. The absorber layer (d) was 2 mm (Fig. 4 left) and 4 mm (Fig. 4 right). It is clear that the reflection-loss peak in the case of samples with the spinel structure (samples S1 and S4) shifts to a lower frequency along with the increased thickness and the peak value becomes bigger and narrower. This shows that by changing the thickness of the material with the spinel structure the position and the attenuation-peak frequency can be easily manipulated in terms of the frequency range. In contrast, the reflection loss for samples with the hexagonal structure (samples S2 and S3) is found to depend sensitively on the absorber thickness in the frequency range from 400 MHz to 32 GHz. These results are in a good agreement with the phenomenon that a decrease in the coercivity may be responsible for the magnetic resonance reduction and as a consequence the thinning of the peaks of the reflection loss (Ghasemi et. al., 2008). We can conclude that composite materials with a larger fraction of the spinel phase/structure can be used as electromagnetic wave absorbers in the lower GHz range, while composite materials with a larger fraction of hexagonal phase might be used in the GHz range above 32 GHz, due to their dielectric and magnetic losses. However, there is a range of compositions that can cover a broad range of frequency absorption, which was the aim of this contribution.

Fig. 15 shows the variation of the reflection loss versus the frequency determined from the composite samples with filler phases (samples S_1–S_4) and two sample thicknesses. The electromagnetic wave absorption data based on Fig. 15 are summarized in Table 5. Here, the bandwidth is defined as the frequency width in which the reflection loss is less than -10 dB, which indicates that 90 % of the EM waves are absorbed by the material (Huo et. al., 2009). RL values of less than -10 dB were obtained with an absorber layer d = 4 in the case of the sample S1 and d = 2 and 4 for the sample S4. It is clear that a wider absorption width of 2.1 GHz and a minimum reflection loss peak of -16.5 dB were observed at 24.8 GHz with an absorber layer of 2 mm for sample S4.
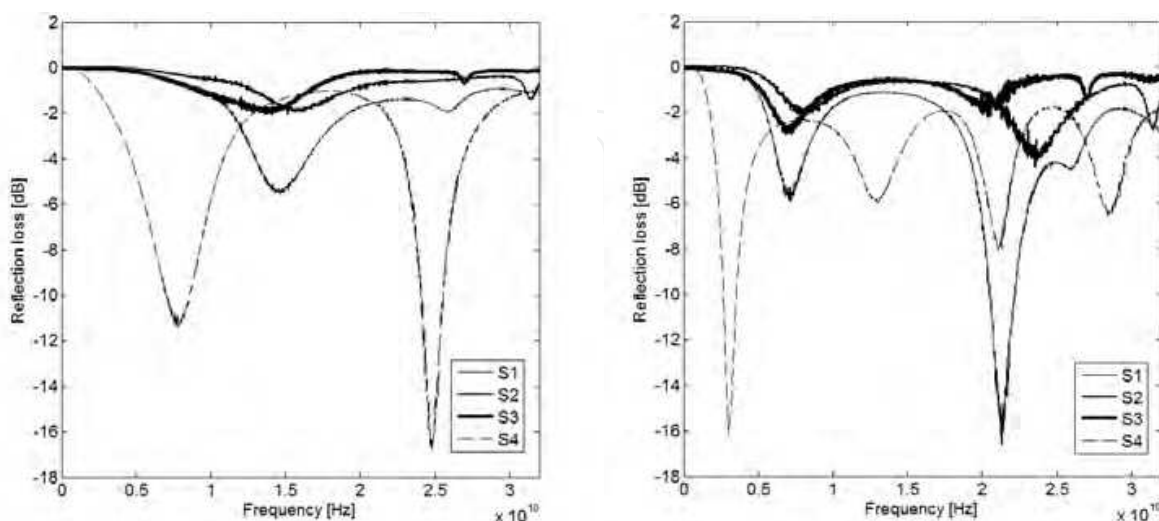

Fig. 15. The dependence of the thickness of absorber layer d (2 mm and 4 mm) on the reflection loss of the composites specimens with weight ratio magnetic-powder: PPS = 80:20.

Samples code	Thickness (mm)	Minimum RL frequency (GHz)	Minimum RL value (dB)
S1	2	14.3	-5.2
	4	7.0	-5.8
		21.3	-16.5
S2	2	15.7	-1.8
	4	7.7	-2.0
		23.5	-4.0
S3	2	14.0	-2.0
	4	7.0	-5.7
		20.5	-2.0
S4	2	7.7	-11.2
		24.8	-16.7
	4	3.0	-16.0
		13.0	-5.8
		21.5	-7.9
		28.5	-6.3

Table 3. Electromagnetic wave absorption properties of composite samples.

3. Conclusions

The microemulsion method is a very adaptable technique which allows the preparation of a different kind of nanomaterials just alone or in combination with other techniques.

In the present investigation γ-Fe_2O_3-SiO_2 core-shell nanoparticles with a narrow particle size distribution were prepared via the precipitation in two different microemulsion systems: water/SDS, 1-butanol/cyclohexane and water/CTAB, 1-butanol/1-hexanol. Results obtained in this research, show that the type of surfactant, concentration of aqueous solution of Fe^{2+}/Fe^{3+} ions, the reaction temperature and the pH value, had a strong influence on average particle size distribution and as a consequence on specific magnetization. Specific magnetization of the γ-Fe_2O_3 nanoparticles is ranging from 14 Am^2/kg for a particle size of 5.6 nm to 60 Am^2/kg for a particle size of 8.8 nm. The specific magnetization of functionalized silica (SiO_2) coated maghemite (γ-Fe_2O_3) nanoparticles sharply decreased due to the non-magnetic nature of SiO_2 layer.

Furthermore, the precursors of the nano-crystalline strontium hexaferrite ($SrFe_{12}O_{19}$) powder were successfully synthesized using the co-precipitation and microemulsion methods. The DTA thermograms indicated an exothermic peak at 719.3 °C for the sample prepared by the co-precipitation method and at 735.1 °C for the sample prepared by the microemulsion method, which could be attributed to an exothermic reaction and the crystallization of the $SrFe_{12}O_{19}$ hexaferrite particles. When using both synthesis methods single-phase $SrFe_{12}O_{19}$ was obtained when the hydroxide precursor prepared at a Sr^{2+}/Fe^{3+} molar ratio of 1:8 was calcined at 900 °C.

The $SrFe_{12}O_{19}$ prepared with Sr^{2+}/Fe^{3+} molar ratios of 1:8 and 1:6.4 had a high saturation magnetization of around 62-64 Am^2/kg and wide hysteresis loops with a coercivity of 5.0-5.4 kOe and remanent magnetization of 36-39 Am^2/kg. Decreasing the Sr^{2+}/Fe^{3+} molar ratio

below 1:8 caused a drastic change in the phase composition and consequently in the shape of the hysteresis loop. Here, the magnetite represents the major phase in the product as a consequence of the self-sintering phenomenon in the reaction mixture, where the iron oxide represents a large part of the constitutive phases.

In the last step we investigated composites designed for microwave absorption based on magnetic filler, composed of phases within the SrO–Fe_2O_3 system, embedded in a polyphenylene sulfide matrix with a concentration ratio of 80:20 by weight. With a manipulation of the molar ratio of Sr^{2+}/Fe^{3+} and a calcination of the co-precipitated precursor at an elevated temperature, one can realize filler within the composite with a multipart crystal structures and multifarious magnetic properties. From this reason it is possible to prepare materials with natural resonance in different frequency ranges. The ferrites with a spinel structure are useful for absorbing materials at lower GHz range while the hexagonal ferrites are special kind of absorbing materials in the range above 32 GHz due to their magnetic anisotropy.

4. References

Ataie A., Harris I.R. & Ponton C.B. (1995). Magnetic properties of hydrothermally synthesized strontium hexaferrite as a function of synthesis conditions, *Journal of Materials Science*, Vol.30, No.6, (June 1995), pp. 1429-1433, ISSN 1573-4803

Bregar V.B. (2004). Potential application of composite with ferromagnetic nanoparticles in microwave absorber, *IEEE Transactions on Magnetics*, Vol.40, No.3, (May 2004), pp. 1679-1684, ISSN 0018-9464

Bregar V.B. & Žnidaršič A. (2006). Analysis of electromagnetic noise suppression in microstrip lines with absorber sheets, *Proceedings of Asia-Pacific Microwave Conference,* pp. 540-543, ISSN: 0018-9464 Yokohama, Japan, December 2006

Bregar V.B. (2004). Potential application of composite with ferromagnetic nanoparticles in microwave absorber, *IEEE Transactions on Magnetics*, Vol.40, No.3, (May 2004), pp. 1679-1684, ISSN 0018-9464

Bregar V.B., Lisjak D., Žnidaršič A. & Drofenik M. (2007). The application of effective-medium theory for the nondestructive characterization of ceramic composites, *Journal of the European Ceramic Society*, Vol.27, No.2-3, (2007), pp. 1071-1076, ISSN 0955-2219

Ding J., Miao W.F., McCormick P.G. & Street R. (1998). High-coercivity ferrite magnets prepared by mechanical alloying, *Journal of Alloys and Compounds,* Vol.281, No.1, (November 1998), pp. 32-36, ISSN 0925-8388

Drofenik M., Ban I., Ferk G., Makovec D., Žnidaršič A., Jagličić Z. & Lisjak D. (2010). The concept of a low-temperature synthesis for superparamagnetic $BaFe_{12}O_{19}$ particles, *Journal of the American Ceramic Society,* Vol.93, No.6, (February 2010), pp. 1602-1607, ISSN 0002-7820

Elvin G., Parkin I.P.P., Bui Q.T., Barquin L.F., Pankhurst Q.A., Komarov A.V. & Morozov Y.G. (1997). Self-propagating high-temperature synthesis of $SrFe_{12}O_{19}$ from reactions of strontium superoxide, iron metal and iron oxide powders, *Journal of Materials Science Letters*, Vol.16, No.15, (January 1997), pp. 1237-1239, ISSN 0261-8028

Feng Y.B., Qiu T. & Shen C.Y. (2007). Absorbing properties and structural design of microwave absorbers based on carbonyl iron and barium ferrite. *Journal of Magnetism and Magnetic Materials,* Vol.318, No.1-2, (2007), pp. 8-13, ISSN 0304-8853

Ghasemi A., Hossienpour A., Morisako A., Liu X. & Ashrafizadeh A. (2008). Investigation of the microwave absorptive behavior of doped barium ferrites, *Materials & design*, Vol.29, No.1, (2008), pp. 112-117, ISSN 0264-1275

Giannakopoulou T., Kompotiatis L., Kontogeorgakos A. & Kordas G. (2002). Microwave behavior of ferrites prepared via sol–gel method, *Journal of Magnetism and Magnetic Materials,* Vol.246, No.3, (May 2002) pp. 360-365(6), ISSN 0304-8853

Groningen R. (November 2003). Magnetic properties of nanocrystaline materials for high frequency applications, *Doctoral dissertation,* ISBN 90 367 1953 4, Netherlands: University of Groningen

Gubin S.P. (1993). *Magnetic nanoparticles,* Edited by: Gubin S.P. © 2009 John Wiley & Sons, ISNB 3527407901, Weinheim

Hessien M.M., Rashad M.M. & El-Barawy K. (2008). Controlling the composition and magnetic properties of strontium hexaferrite synthesized by co-precipitation method, *Journal of Magnetism and Magnetic Materials,* Vol.320, No.3-4, (February 2008), pp. 336–343, ISSN 0304-8853

Huo J., Wang L. & Yu H. (2009). Polymeric nanocomposites for electromagnetic wave absorption, *Journal of Materials Science,* Vol.44, No.15, (2009), pp. 3917-3927, ISSN 0022-2461

Kadama R.H., Berkowitz A.E., McNiff E.J. & Foner S. (1996). Surface spin disorder in $NiFe_2O_4$, *Physical Review Letter,* Vol.77, No.2, (July 1996), pp. 394-397, ISSN 0031-9007

Kim S., Han D. & Cho S. (1994). Microwave absorbing properties of sintered Ni-Zn ferrite, *IEEE Transactions on Magnetics,* Vol.30, No.6, (November 1994), pp. 4554-4556, ISSN 0018-9464

Košak A., Makovec D. & Drofenik M. (2004). The preparation of MnZn-ferrite nanoparticles in a water/CTAB, 1-butanol/1-hexanol reverse microemulsion, *Physica status solidi (c),* Vol.1, No.12, (December 2004), pp. 3521-3524, ISSN 1610-1634

Košak A., Makovec D., Drofenik D. & Žnidaršič A. (2004). In situ synthesis of magnetic MnZn-ferrite nanoparticles using reverse micro emulsion, *Journal of Magnetism and Magnetic Materials,* Vol. 272-276 (2004), pp. 1542-1544, ISSN 0304-8853

Lax B. & Button K.J. (1962). *Microwave Ferrites and Ferrimagnetics,* Edited by : McGraww-Hill, ISBN 62011947, New York

Makovec D. & Košak A. (2005). The synthesis of spinel–ferrite nanoparticles using precipitation in microemulsions for ferrofluid applications, *Journal of Magnetism and Magnetic Materials,* Vol.289, (March 2005), pp. 32-35, ISSN: 0304-8853

Mornet S., Grasset F., Portier J. & Duguet E. (2002). Maghemite@silica nanoparticles for biological applications, *European Cells and Materials,* Vol.3, No.2, (2002), pp. 110-113, ISSN 1473-2262

Nakamura T. & Hankui E. (2003). Control of high-frequency permeability in polycrystalline (Ba,Co)-Z-type hexagonal ferrite. *Journal of Magnetism and Magnetic Materials,* Vol.257, No.2-3, (February 2003), pp. 158-164, ISSN 0304-8853

Natarajan U., Handique K., Mehra A., Bellare J.R. & Khilar K.C. (1996). Ultrafine metal particle formation in reverse micellar systems: effects of intermicellar exchange on

the formation of particles, Langmuir, Vol.12, No.11, (May 1996), pp. 2670–2678, ISSN 0743-7463

Ni S., Sun X., Wang X., Zhou G., Yang F., Wang J. & He D. (2010). Low temperature synthesis of Fe_3O_4 micro-spheres and its microwave absorption properties, Materials Chemistry and Physics, Vol.124, No.1, (November 2010), pp. 353-358, ISSN 0254-0584

Ovtar S., Lisjak D. & Drofenik M. (2011) Preparation of oriented barium hexaferrite films by electrophoretic deposition. Journal of the American Ceramic Society, [in press, accepted manuscript].

Pankov V.V., Pernet M., Germi P. & Mollard P. (1993). Fine hexaferrite particles for perpendicular recording prepared by the co-precipitation method in presence of an inert component, Journal of Magnetism and Magnetic Materials, Vol.120, No.1-3, (1993) 69-72, ISSN 0304-8853

Pardavi Horvath M. (2000). Microwave application of soft ferrites. Journal of Magnetism and Magnetic Materials, Vol.215-216, No.1, (December 2000), pp. 171-183, ISSN 0304- 8853

Pereira F.M.M., Santos M.R.P., Sohn R.S.T.M., Almeida J.S., Medeiros A.M.L., Costa M.M. & Sombra A.S.B. (2009). Magnetic and dielectric properties of the M-type barium strontium hexaferrite $(Ba_xSr_{1-x}Fe_{12}O_{19})$ in the RF and microwave (MW) frequency range, Journal of Materials Science: Materials and Electronics, Vol.20, No.5, (2009), pp. 408-417, ISSN 0957-4522

Rezlescu L., Rezlescu E., Popa P.D. & Rezlescu N. (1999). Fine barium hexaferrite powder prepared by the crystallisation of glass. Journal of Magnetism and Magnetic Materials, Vol. 193, No. 1-3, (March 1999), pp. 288-290, ISSN 0304-8853

Rodrigue G.P. (1963). Magnetic materials for millimeter applications. IEEE Transactions on Microwave Theory and Techniques, Vol.MMT-11 pp. 351-356

Sato H. & Umeda T. (1993). Grain Growth of Strontium Ferrite Crystallized from Amorphous Phases, Materials Transactions, JIM, Vol.34, No.1, (January 1993), pp. 76-8, ISSN 0916-1821

Schieber M.M. (1976). Experimental Magnetochemistry, in: Selected Topics in Solid State Physics, vol. VIII, ed. E.P. Wohlfarth, North-Holland, Amsterdam

Surig C., Hempel K.A. & Bonnenberg D. (1994). Hexaferrite particles prepared by sol-gel technique, IEEE Transactions on Magnetics, Vol.30, No.6, (November 1994), pp. 4092-4094, ISSN 0018-9464

Urek S. & Drofenik M. (1996). Influence of iron oxide reactivity on microstructure development in MnZn ferrites, Journal of Materials Science, Vol.31, No.18, (1996) 4801-4805, ISSN 0022-2461

Verma A., Mendiratta R.G., Goel T.C. & Dube D.C. (2002). Microwave studies on strontium ferrite based absorbers. Journal of Electroceramics, Vol. 8, No. 3, (September 2002), pp. 203-208, ISSN 1385-3449

Vidal-Vidal J., Rivas J. & López-Quintela M.A. (2006). Synthesis of monodisperse maghemite nanoparticles by the microemulsion method, Colloids and Surfaces A: Physicochemical and Engineering Aspects, Vol.288, No.1-5, (October 2006), pp. 44-51, ISSN 0927-7757
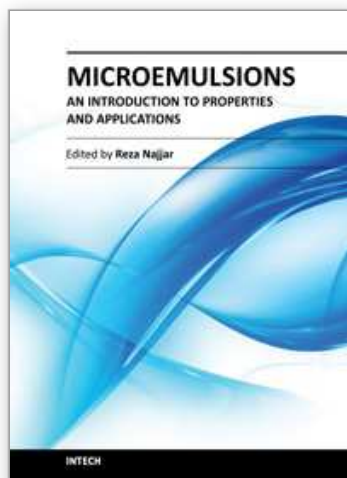
Microemulsions - An Introduction to Properties and Applications

Edited by Dr. Reza Najjar

The rapidly increasing number of applications for microemulsions has kept this relatively old topic still at the top point of research themes. This book provides an assessment of some issues influencing the characteristics and performance of the microemulsions, as well as their main types of applications. In chapter 1 a short introduction about the background, various aspects and applications of microemulsions is given. In Part 2 some experimental and modeling investigations on microstructure and phase behavior of these systems have been discussed. The last two parts of book is devoted to discussion on different types of microemulsion's applications, namely, use in drug delivery, vaccines, oil industry, preparation of nanostructured polymeric, metallic and metal oxides materials for different applications.

How to reference

In order to correctly reference this scholarly work, feel free to copy and paste the following:

A. Drmota, M. Drofenik, J. Koselj and A. Žnidaršič (2012). Microemulsion Method for Synthesis of Magnetic Oxide Nanoparticles, Microemulsions - An Introduction to Properties and Applications, Dr. Reza Najjar (Ed.), ISBN: 978-953-51-0247-2, InTech, Available from: http://www.intechopen.com/books/microemulsions-an-introduction-to-properties-and-applications/microemulsion-method-for-synthesis-of-magnetic-oxide-nanoparticles

INTECH

open science | open minds